ECS Transactions, 45 (5) 11-19 (2012)
10.1149/1.3700405 ©The Electrochemical Society

Growing Si Nanocrystals within *a*-Si Nanoclusters Embedded in *a*-SiO_2: Evolution of Photoluminescence

L.J. Borrero-González[a], L.A.O. Nunes[a], F.E.G. Guimarães[a], J Wojcik[b], P Mascher[b], A.M. Gennaro[c], M. Tirado[d] and D. Comedi[e,f]

[a]Instituto de Física de São Carlos, Universidade de São Paulo, CP 369, 13560-970, São Carlos, SP, Brazil
[b]Department of Engineering Physics and Centre for Emerging Device Technologies, McMaster University, Hamilton, Ontario L8S 4K1, Canada
[c]INTEC (CONICET-UNL), Güemes 3450, 3000 Santa Fe, Argentina, and Departamento de Física, Facultad de Bioquímica y Ciencias Biológicas, Universidad Nacional del Litoral, Ciudad Universitaria, 3000 Santa Fe, Argentina
[d]LPDM and [e]LAFISO, Dep. de Física, Facultad de Ciencias Exactas y Tecnología, Univ. Nacional de Tucumán, Av. Independencia 1800, S. M. de Tucumán, 4000 Argentina
[f]CONICET, Argentina

We combine X-ray absorption, electron spin resonance and Raman spectroscopies, X-ray diffraction and photoluminescence (PL) techniques to determine the structure and luminescence mechanisms in Si nanoclusters (Si-ncls) embedded within Si oxides at various intermediate formation stages. The Si-ncls/oxide systems are fabricated by thermally annealing plasma-enhanced chemical vapor deposited Si-rich Si-oxide films. The structural and chemical orders in the amorphous oxide matrix, the Si-ncls amorphous and crystalline volume fractions and sizes, the dangling bond density and PL spectra and decay rates are followed closely as a function of the annealing temperature. The results can be interpreted by a crystalline core/amorphous shell model for the Si-ncls. The important role of the shell, often ignored in the literature, is discussed. As the Si-ncls crystalline cores grow at the expense of thinning amorphous shells, the PL undergoes a transition from a regime dominated by disorder-induced effects to a situation where quantum confinement prevails.

Introduction

Luminescent Si nanoclusters (Si-ncls) embedded in amorphous silicon oxides obtained by thermal annealing of Si-rich Si-oxides have been studied for many years due to their potential application in Si-photonics. However, the specific origin of the luminescence from real systems is still matter of active discussion in the literature (1,2). Much of the controversy on this respect probably stems from the inherent complexity of the chemically and structurally disordered amorphous oxide matrix and Si-ncl/matrix interfaces, which are seldom characterized or properly controlled in the experiments.

In this invited paper, we describe our recent efforts to improve the characterization and understanding of the luminescence from Si-ncls embedded in amorphous Si oxides.

We combine synchrotron X-ray absorption spectroscopy (XAS) and electron spin resonance (ESR) experiments with Raman spectroscopy, X-ray diffraction (XRD) and photoluminiscence (PL) techniques to determine the structure, paramagnetic defect status and luminescence mechanisms in Si-ncls/oxide composite systems at various intermediate formation stages within Si-rich Si oxide (SRSO) films having different Si concentrations (y = 0.36-0.45, where y is defined as the Si concentration in Si_yO_{1-y}), fabricated by plasma-enhanced chemical vapor deposition methods and isochronally (2h) annealed at various temperatures (T_a = 900-1100 ºC) under either Ar or (Ar+5%H_2) atmospheres (2,3).

Experimental Details

2 μm thick SRSO films with various Si concentrations (y = 0.36-0.45 in Si_yO_{1-y}) were deposited on fused quartz and (100) Si substrates by electron-cyclotron resonance or inductively-coupled plasma-enhanced chemical vapor deposition. The substrate temperature during the depositions was typically 120 ºC. After the growths the films were annealed under Ar or (Ar+5%H_2) at either 900, 1000 or 1100 ºC for two hours to promote different stages of Si-ncl formation in an amorphous Si oxide matrix, as described elsewhere (4,5). Some samples on Si substrates were studied by XAS and X-ray excited optical luminiscence (XEOL) at the Spherical Grating Monochromator (SGM) beamline of the Canadian Light Source (CLS) Synchrotron Facility. The y values were determined by Rutherford backscattering RBS measurements for samples prepared on both *c*-Si and glassy carbon substrates. ESR measurements were performed at room temperature on films deposited on quartz substrates, using a Bruker ER-200 spectrometer working at 9.375 GHz (X band). Microwave power was set at 2 mW, and the modulation frequency was 100 kHz with modulation amplitude of 0.32 mT. The films on quartz were studied by PL (CW) and time-resolved PL spectroscopy. The PL spectra were recorded by using an HR4000 Ocean Optics spectrometer as a detection system. The 442 nm line of a He–Cd laser was used as the excitation source. The decay kinetics of the luminescence were studied using the second harmonic of a Q-switched neodymium-doped yttrium aluminium garnet (Nd:YAG) laser (532 nm, 6 Hz repetition rate) as the source of excitation.

Results and Discussion

XRD: oxide ordering and Si-ncl cystallization

Fig. 1(a) shows XRD scans obtained for as-grown *a*-Si_yO_{1-y} films with y=0.40, 0.42 and 0.45 and for the Si substrate used for the depositions. A very broad peak appears at about 23^o due to the *a*-Si_yO_{1-y} film that becomes narrower as y is decreased. We interpret this peak as the first scattering peak (FSP) of the *a*-Si_yO_{1-y} structure. It is well known from infrared spectroscopy studies (6) that, in the absence of clustering, PECVD-grown *a*-Si_yO_{1-y} films can be nearly characterized by statistical distributions of $Si\text{-}O_{4-n}Si_n$ (n=0,1,2,3,4) tetrahedra whose relative concentration depends on y (the random bonding model (7)). As y is reduced from y=0.5, an increasing contribution from low n tetrahedra and a narrowing of the statistical distribution are expected. The y=1/3 limit corresponds to *a*-SiO_2 where a sharp distribution at n=0 should occur. The narrowing of the FSP as y

is decreased from 0.45 to 0.40 [Fig. 1(a)] indicates a corresponding improved ordering of the amorphous lattice, which could be related to the sharpening of the tetrahedra distribution.

Fig. 1(b) shows typical XRD data for annealed *a*-Si_yO_{1-y}. As the annealing temperature is increased, Si nanocrystals form within an amorphous oxide matrix, as indicated by the emergence of the Si peak at ~28.4° and the FSP. The Si (220) and (331) peaks are also observed (4) at 47.3° and 56.1° (data not shown) which confirms the crystallization of Si regions. From the width of the Si (111) peak (4), the mean size of the crystalline Si clusters is estimated to grow up to ~ 4.5 - 8 nm at 1100°C, the larger sizes corresponding to samples with larger *y*. The oxide phase, in contrast, is still amorphous (the crystallization temperature of *a*-SiO_2 is above 1400°C) and is characterized by the FSP, which gradually shifts to lower diffraction angles and narrows as T is increased [see Fig. 1(b)].

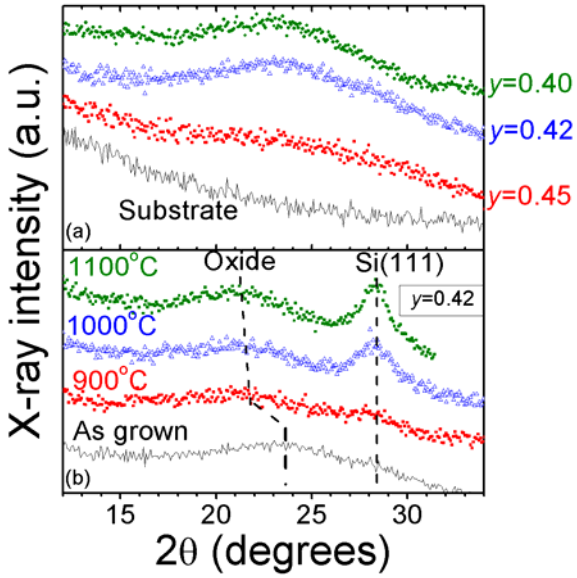

Figure 1. XRD scans as obtained for (a) a c-Si substrate (line) and as grown *a*-Si_yO_{1-y}: *y*=0.40 (squares), 0.42 (triangles) and 0.45 (circles); and (b) *a*-$Si_{0.42}O_{0.58}$: as grown (line) and annealed at 900°C (circles), 1000°C (triangles) and 1100°C (squares). The Si (111) and oxide first scattering peak (FSP) are indicated in (b).

The shift to lower angles reflects an increase of the period of the atomic fluctuations associated to medium range order (MRO) in the oxide. The FSP observed for *a*-SiO_2 close to 21.5° has been shown to mimic the reflection from {111} planes from β-cristobalite quartz (period of 0.411 nm (8)). The FSP peak for *a*-Si, on the other hand, mimics the Si (111) peak of crystalline Si (period of 0.313 nm (9)). Hence, we tentatively interpret the shift to lower angles of the FSP in annealed *a*-Si_yO_{1-y} as a gradual transition of a substoichiometric oxide alloy (characterized mainly by mixed Si-$O_{4-n}Si_n$ tetrahedra with n=1,2,3) to the stoichiometric *a*-SiO_2 (Si-O_4 tetrahedra). Such an alloy regime with oxidation states of Si lower than +4 characterizes the Si/SiO_2 planar interface (10) and the transition from it into Si-O_4 and Si-Si_4 has indeed been observed in *a*-Si_yO_{1-y} by high-resolution photoelectron (11) and infrared spectroscopy (6). The period of quasi-Bragg

planes in the alloy phase should be some weighted average of 0.411 and 0.313 nm and approach the value of 0.411 nm as the *a*-SiO_2 phase is chemicaly ordered.

The XRD scans of annealed *a*-Si_yO_{1-y} were background corrected and the oxide FSP and the Si (111) peak were satisfactorily fit by the sum of two Lorentzians, as in Ref. (4). This procedure was systematically applied to all the XRD curves obtained and enabled us to consistently determine the FSP positions [Fig. 2(a)] and widths [Fig. 2(b)] for the as grown and annealed samples as a function of the annealing temperature. It can be seen that already at T=900°C, the FSP position has undergone a significant shift towards lower diffraction angles with respect to the FSP in the as grown samples, while the FSP width has remained essentially unchanged. This effect indicates that at T = 900°C, the oxide has undergone significant chemical ordering, while the correlation length that characterizes MRO has not changed much. The strong chemical ordering at 900°C is consistent with previous studies (6). For T>900°C, the FSP position continues to decrease as the oxide continues to approach the stoichiometric limit. In this region, the width also decreases significantly, indicating a significant gradual improvement of the MRO (i.e. increase of the coherence length). The scatter of the present data and a small variation in *y* does not permit us to discuss conclusively trends with composition at this stage.

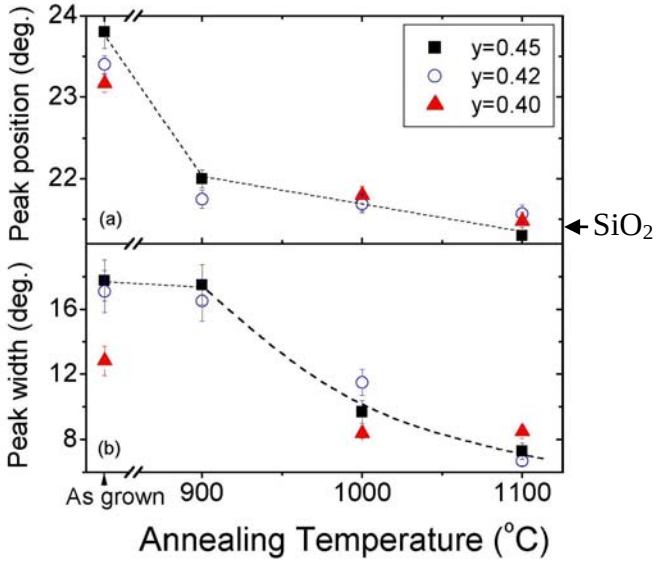

Figure 2. (a) Position, and (b) width of the Si oxide first scattering peak (FSP) in a 2θ scale as deduced from the least square fit of two Lorentzians to the diffraction data for as grown and annealed *a*-Si_yO_{1-y} samples (*y*=0.40, 0.42 and 0.45), as a function of the annealing temperature. The dashed lines are meant to guide the eye through the data points for the y=0.45 sample. The FSP position reported in the literature for stoichiometric SiO_2 (8) is indicated by an arrow on the left of (a).

XAS and ESR: amorphous Si-ncls already exist in the as grown Si oxide

Our XAS data, however, show that amorphous Si regions exist within the as-deposited amorphous, chemically disordered, Si oxide films. Figure 3 shows the X-ray absorbance spectrum of the Si K-shell edge for a Si_yO_{1-y} film with *y*=0.40 (as grown and annealed at 900ºC and 1100ºC). In addition to the strong peak around 1847 eV due to Si-O_4 tetrahedra (which corresponds to the regular chemical environment in pure SiO_2),

important contributions from mixed Si-$O_{4-n}Si_n$ tetrahedra with n=1,2,3 are observed for lower energies down to 1840 eV, where a significant shoulder corresponding to Si-Si_4 is also present in the unannealed sample. An analysis indicates that most of the excess silicon is already precipitated into amorphous nanoclusters in the as grown film (2). The strong chemical ordering tendency deduced by XRD after annealing at T_a = 900 °C and 1100ºC is confirmed by the XAS data, as deduced by the reduced contributions from the mixed tetrahedra and the concomitant increase in the SiO_4 peak in the spectrum of Fig. 3. For T_a=1000 and 1100ºC, this trend is accompanied by a reduction of the Si dangling bond density, as determined from the ESR data (2), and an increase of the crystalline Si volume fraction, as deduced from XRD and Raman (3).

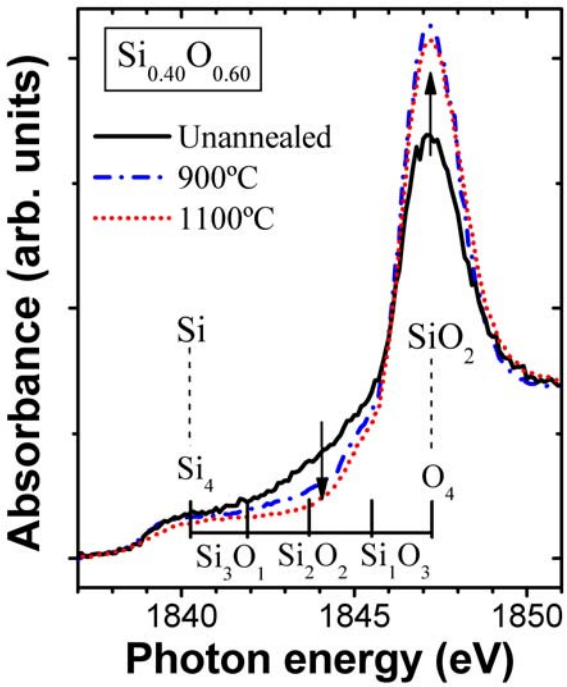

Figure 3. X-ray absorbance versus synchrotron X-ray energy for Si_yO_{1-y} films with y=0.40 (as grown and annealed at 900ºC and 1100ºC in Ar+5%H_2). The peak positions for different possible atomic tetrahedra around Si atoms in the samples are indicated.

Structural model:

To explain these results, we propose crystallization by nucleation within already existing amorphous Si-ncls as the mechanism for the formation of the Si nanocrystals in the oxide matrix. The cluster-size dependent partial crystallization of Si-ncls at intermediate T_a can be qualitatively understood in terms of a “crystalline core-amorphous shell” Si-ncl model. This is shown schematically in Fig. 4. As the crystalline core grows at the expense of a thinning amorphous shell with increasing T_a, Si dangling bonds in the disordered Si region annihilate, while the MRO in the oxide increases.

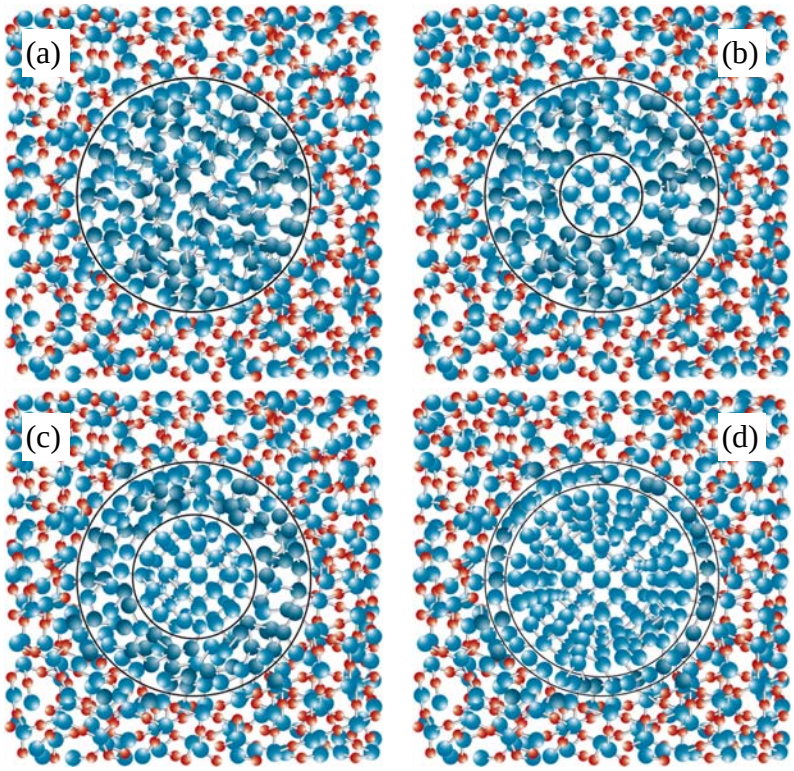

Figure 4. Schematic description of structural model deduced from the XRD, Raman, ESR and XAS data: (a) the as-grown oxide exhibits very poor medium range order, strong chemical disorder and embedded fully amorphous Si nanoclusters; (b) after annealing at T_a > 900ºC the oxide exhibits greatly improved chemical order and crystalline nuclei are spontaneously formed within the amorphous Si clusters; (c,d): for T_a = 1000ºC and 1100ºC, the crystalline core grows at the expense of the thinning amorphous Si shell, while the oxide's medium range order is greatly improved (2).

Photoluminescence:

Typical results of time dependent PL measurements are shown in Figure 5. The inset shows a representative PL spectrum, which is a broad band due to the polydispersity of the Si-ncl emitters within the oxide (5). The decay curves can be well fit by stretched exponentials, as shown. The determined decay rates, $1/\tau$, are clearly a function of the PL detection energy for this case (12).

We find a very distinct PL behavior on samples having disordered Si-ncls (i.e. annealed at 900ºC) as compared to those exhibiting nearly crystalline Si-ncls (i.e. annealed at 1100ºC): while for the latter the PL decay rate shows strong emission wavelength dispersion (as shown in Figure 5), for samples having disordered Si-ncls the PL decay rate dispersion are very small or null (2, 3).

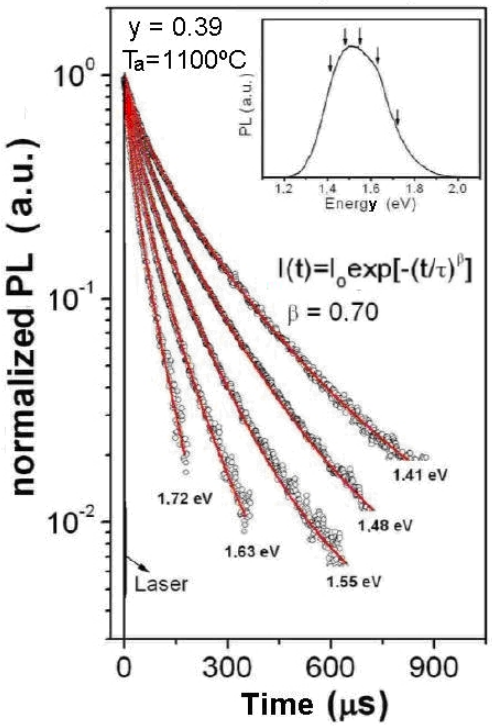

Figure 5. PL time decay curves measured for various PL detection energies for a Si_yO_{1-y} film with y=0.39 annealed at T_a=1100ºC for 2h in (Ar+5%H_2). The red solid lines through the data points are fits of a stretched exponential function with fixed exponent β=0.70 and decay rate 1/τ adjusted so as to fit the data. The inset shows the PL spectrum and the detection energies chosen to measure the decay curves (12).

Figure 6 shows the PL decay rate for different detection energies (E_{det}) as function of the temperature for a Si_yO_{1-y} film with y=0.39. Although the decay rate is found to increase with increasing temperature for the three annealing temperatures considered, it is clear that the E_{det} dispersion is absent for T_a=900ºC (Figure 6(a)) while it is mostly pronounced for T_a= 1100ºC (Figure 6(c)). Indeed, for the latter the total decay rate increases strongly with E_{det} indicating a confinement effect. Furthermore, the corresponding data sets can be well fit by an exciton two-level model (red solid lines in Figure 6), where the triplet-singlet exchange energy and the triplet radiative rate both increase with E_{det}, as expected from quantum confinement (12). For T_a=900ºC, in contrast, for which the Si-ncls are amorphous, no dispersion is observed and the experimental data points cannot be well fit by the quantum confined exciton model. More effects showing the same trend have been reported in previous papers (2, 3).

We attribute these effects to disorder-induced decoherence and/or localization of the excitonic wave function in the amorphous Si-ncls, which diminish the quantum confinement and reinforce disorder-induced breakdown of the k-selection rule effects. It should be noted that the amorphous shell, which is invisible in most diffraction and electron microscopy experiments, should have an important impact on light emission. This is because the amorphous/crystalline interface is not a confining interface and the exciton wavefunction can penetrate the amorphous region. Hence, the full (amorphous shell + crystalline core) Si-ncl size should be considered when estimating the confinement size, not just the crystalline core size that is usually observed in electron microscopy or X-ray diffraction experiments. This rationale puts a question mark on

hypothetical luminescent interface states often invoked to explain the observed partial pinning of the emission energy with decreasing nanocrystal size in similar systems.

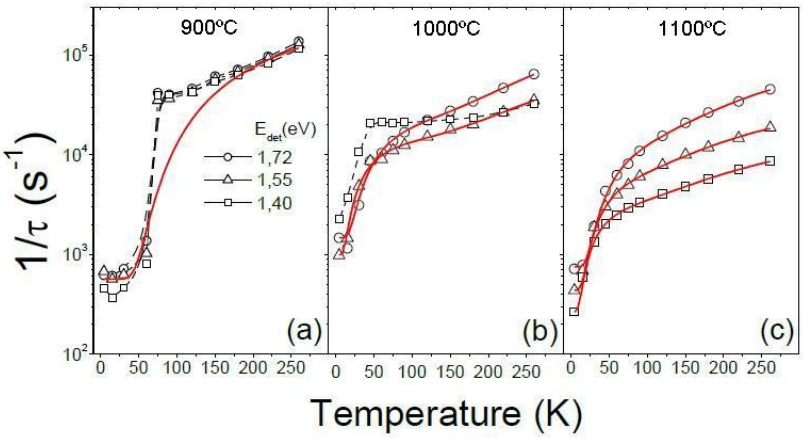

Figure 6. PL decay rates for three different PL detection energies deduced for a Si_yO_{1-y} film with y=0.39 annealed in Ar+5%H_2 at 900ºC (a), 1000ºC (b) and 1100ºC (c) for 2 h. Dashed lines are guides to the eyes. Red solid lines are best fits of a model that includes quantum confined exciton radiative recombination and multiphonon non-radiative recombination (12).

Conclusions

Based on XAS, XRD, ESR and Raman data, a realistic description of Si nanoclusters and the embedding oxide at various formation stages is given. The overall analysis of the optical and structural data indicates that, as the Si-ncl crystalline core grows at the expense of a thinning amorphous shell with increasing T_a, the PL undergoes a transition from a regime dominated by disorder-induced effects to a situation where quantum confinement of excitons prevails.

Acknowledgments

We acknowledge financial support through the Inter American Collaboration in Materials (CIAM) initiative, from the Brazilian Agencies CNPq and FAPESP, the Argentinean CONICET and The Academy of Sciences for the Developing World (TWAS). The work at McMaster University is supported by the Natural Sciences and Engineering Research Council (NSERC), the Canadian Institute for Photonic Innovation (CIPI) and the Centre for Photonics of Ontario Centres of Excellence, Inc. DC and AMG are members of the research career of CONICET, Argentina.

References

1. S. Godefroo, M. Hayne, M. Jivanescu, A. Stesmans, M. Zacharias, O.I. Lebedev, G. Van Tendeloo and V.V. Moshchalkov, *Nature Nanotech.,* **3**, 174 (2008).
2. L.J. Borrero-González, L.A.O. Nunes, F.E.G. Guimarães, J Wojcik, P Mascher, A.M. Gennaro, M. Tirado and D. Comedi, *J. Phys. Condens. Matter*, **23**, 505302 (2011).
3. L.J. Borrero-González, L.A.O. Nunes, M.R.B. Andreeta, J. Wojcik, P. Mascher, Y.A. Pusep, D. Comedi, F.E.G. Guimarães, , *J. Appl. Phys.*, **108**, 13105 (2010).
4. D. Comedi, O.H.Y. Zalloum, E.A. Irving, J. Wojcik, T. Roschuk, M.J. Flynn and P. Mascher *J. Appl. Phys.,* **99** 023518 (2006).
5. D. Comedi, O.H.Y. Zalloum, J. Wojcik, and P. Mascher, *IEEE J. Sel. Top. Quantum Electron.,* **12** 1561 (2006).
6. G. Lucovsky, *J. Non-Cryst. Solids*, **227-230**, 1 (1998).
7. H.R. Philipp, *J. Phys. Chem. Solids*, **32**, 1935 (1971).
8. P.H. Gaskell and D.J. Wallis, *Phys. Rev. Lett.*, **76**, 66 (1996).
9. A.H. Mahan, J. Yang, S. Guha, and D.L. Williamson, *Phys. Rev. B,* **61**, 1677 (2000).
10. F.J. Himpsel, F.R. McFeely, A. Taleb-Ibrahimi, J.A. Yarmoff, and G. Hollinger, *Phys. Rev. B,* **38**, 6084 (1988).
11. T.P. Chen, Y. Liu, C.Q. Sun, M.S. Tse, J.H. Hsieh, Y.Q. Fu, Y.C. Liu, and S. Fung, *J. Phys. Chem. B,* **108**, 16609 (2004).
12. L. Borrero, PhD Thesis, IFSC, São Paulo University, São Carlos, Brazil (2010).